

Photon-hadron and photon-photon collisions in ALICE

Rainer Schicker, for the ALICE Collaboration

Physikalisches Institut, Im Neuenheimer Feld 226, 69120 Heidelberg

E-mail: schicker@physi.uni-heidelberg.de

Abstract.

A review is given on photon-hadron and photon-photon collisions in the ALICE experiment. The physics motivation for studying such reactions is outlined, and the results obtained in proton-lead and lead-lead collisions in Run 1 of the LHC are discussed. The improvement in detector rapidity coverage due to a newly added detector system is presented. The ALICE perspectives for data taking in LHC Run II are summarised.

1. Introduction

The ALICE experiment consists of a central barrel and of a forward muon spectrometer[1]. Additional detectors are installed outside of the central barrel for trigger and event classification purposes. The excellent particle identification capabilities of the central barrel, in conjunction with the low magnetic field, allow ALICE to investigate a variety of exclusive reaction channels as occurring in photon-hadron and photon-photon collisions[2]. Here, the exclusivity of the particles produced within the central barrel can be imposed by requiring no signal in the detectors outside of the central barrel. The ALICE collaboration has taken data from 2010 to 2013 in proton-proton, proton-lead and lead-lead collisions during Run I at the LHC. In the shut-down period 2013-2015 between Run I and Run II, a new detector system ADA/ADC was installed. This new detector covers additional two units of pseudorapidity on both sides of the central barrel, and hence contributes to an improved exclusivity condition of the analysed events, and to an improved recognition of beam-gas background events.

2. Photon-photon collisions

Heavy-ion beams are the source of strong electromagnetic fields. In the Equivalent Photon Approximation (EPA), these fields are represented by an ensemble of equivalent photons[3, 4]. The cross section of heavy-ion induced photon-photon processes can be expressed as

$$\sigma_{PbPb \rightarrow PbPb X}^{EPA} = \int \int dn_{1,\gamma} dn_{2,\gamma} \sigma_{\gamma\gamma \rightarrow x}(\omega_1 \omega_2), \quad (1)$$

with $dn_{1,\gamma}$, $dn_{2,\gamma}$ the photon flux in leading log. approximation of beam 1 and 2, respectively:

$$dn_{\gamma}(\omega, b) = \frac{Z^2 \alpha}{\pi^2} \frac{d\omega}{\omega} \frac{d^2b}{b^2}. \quad (2)$$

In Eq. 2, the photon flux is given differentially in the photon energy ω and the impact parameter b of the two colliding heavy ions. The photon-photon luminosity in EPA formalism is expressed in leading log. approximation as

$$\frac{dL}{dWdy} = \frac{2}{W} \frac{dL}{d\omega_1 d\omega_2} = \frac{2}{W} \frac{dn_1(\omega_1)}{d\omega_1} \frac{dn_2(\omega_2)}{d\omega_2} = \frac{4Z^4\alpha^2}{\pi^2(\omega_1\omega_2)^{3/2}} \log\left(\frac{\gamma}{R\omega_1}\right) \log\left(\frac{\gamma}{R\omega_2}\right), \quad (3)$$

with the invariant mass $W=2\sqrt{\omega_1\omega_2}$ and the rapidity $y=\frac{1}{2}\log\left(\frac{\omega_1}{\omega_2}\right)$ of the two-photon system. Here, ω_1 and ω_2 denote the energies of the two interacting photons.

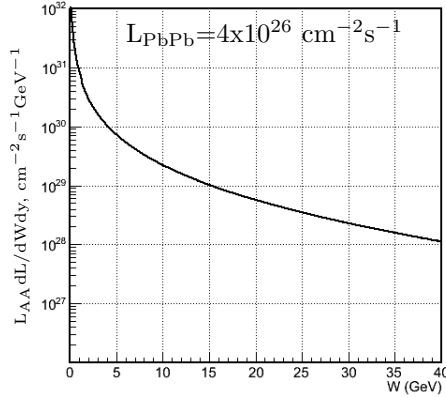


Figure 1. Photon-photon luminosity for Pb-Pb at $\sqrt{s_{NN}} = 5.18$ TeV.

Shown in Figure 1 is the photon luminosity $L_{AA} \frac{dL}{dWdy}$, calculated for a Pb-Pb luminosity of $L_{AA} = 4 \times 10^{26} \text{ cm}^{-2} \text{ s}^{-1}$ and a center-of-mass energy of $\sqrt{s_{NN}} = 5.18$ TeV.

3. Photon-hadron collisions

The photons of the electromagnetic field of one nucleus can interact with a nucleus of the other beam, and can initiate a variety of photon-hadron reactions. Of particular interest here is the process of exclusive vector-meson photoproduction[5].

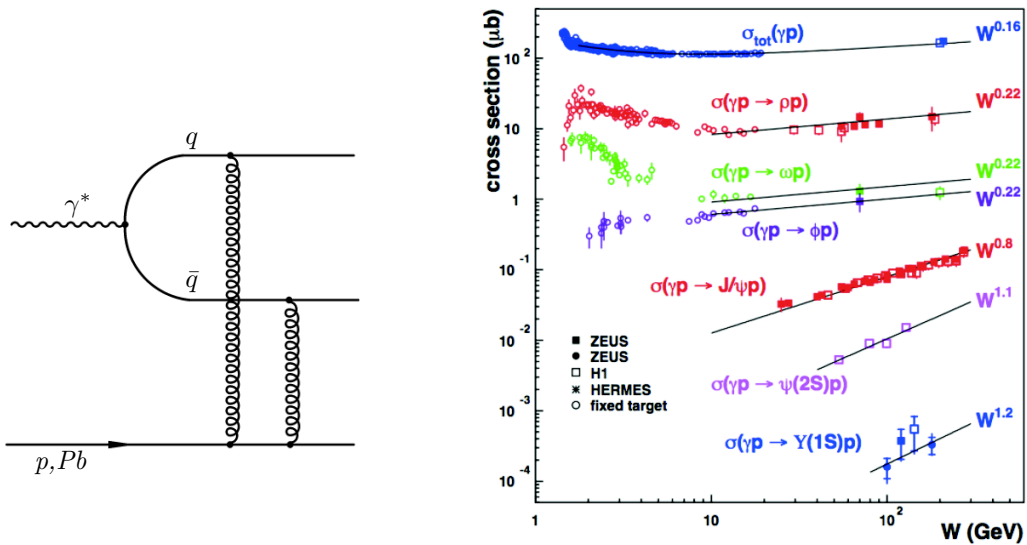


Figure 2. Vector-meson photoproduction diagram on left, energy dependence of cross section on the right (Figure taken from [6]).

The Feynman diagram for photoproduction of a vector-meson is shown in Figure 2 on the left. The incoming photon fluctuates into a $q\bar{q}$ -excitation and gets scattered on-shell by the interaction. This interaction is due to colour-singlet exchange of gluons, hence is of diffractive nature. The systematic study of this process for vector-mesons of different masses, for low and high values of t (t = four momentum transfer) and for low and high Q^2 (Q^2 = photon virtuality), allows to study the nature of diffractive processes at a soft and hard scale, and in the transition region in between. In the analysis of the J/ψ cross section from HERA data, it was found that hard pomeron exchanges need to be included to get agreement with the data. This hard pomeron contribution also significantly improves the Regge fits of the ρ -production cross section at high t -values [7]. Figure 2 on the right shows the photoproduction cross section for vector-mesons of different masses as function of the photon-proton center-of-mass energy W . Clearly visible is the weak energy dependence for the light mass of the ρ , and the much steeper energy dependence for the heavy masses of the J/ψ and Υ .

The mass of the J/ψ introduces a relatively hard scale, and hence allows a perturbative QCD description. The amplitude can be factorized in lowest order into the amplitude of the $\gamma \rightarrow c\bar{c}$ transition, the colour-singlet gluonic interaction of the $c\bar{c}$ -system with the proton, and the evolution of the $c\bar{c}$ -system into the J/ψ , resulting in a cross section of

$$\frac{d\sigma}{dt}(\gamma^*p \rightarrow J/\psi p)|_{t=0} = \frac{\Gamma_{ee} M_{J/\psi}^3 \pi^3}{48\alpha} \left[\frac{\alpha_s(\bar{Q}^2)}{\bar{Q}^4} xg(x, \bar{Q}^2) \right]^2 \left(1 + \frac{Q^2}{M_{J/\psi}^2} \right). \quad (4)$$

The cross section for J/ψ -photoproduction is shown in Eq. 4. This cross section depends on the integrated gluon distribution $xg(x, Q^2)$ squared, and hence allows the study of this gluon distribution at low x -values [8]. The analysis of this process on a Pb-nucleus gives access to the nuclear gluon distribution, and is interesting for investigating nuclear medium effects.

4. The ALICE experiment

In the ALICE central barrel, the information from the Inner Tracking System (ITS), the Time Projection Chamber (TPC) and the Time-of-Flight system (TOF) allows momentum reconstruction and particle identification in the pseudorapidity range $-0.9 < \eta < 0.9$. A muon spectrometer covers the pseudorapidity range $-4. < \eta < -2.5$ [1].

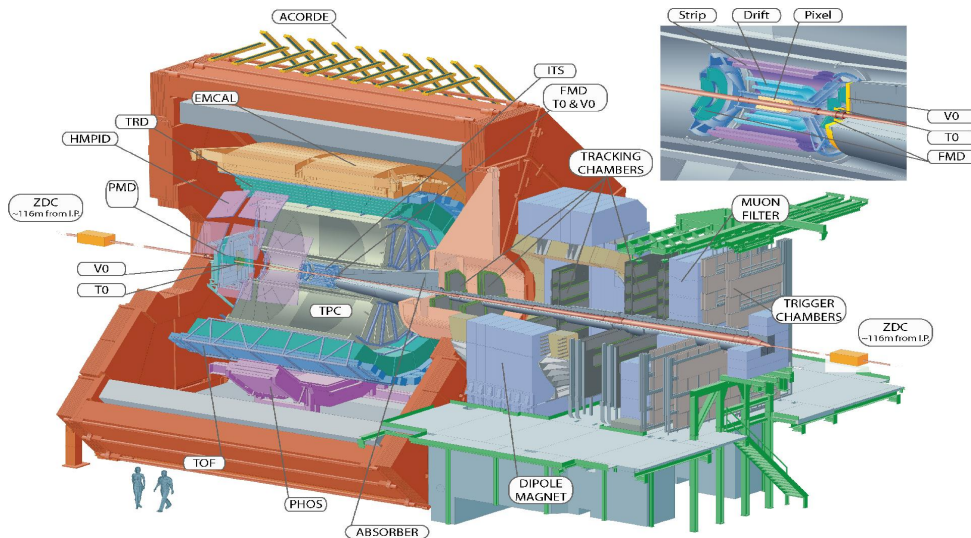


Figure 3. The ALICE experiment.

The different detector systems of the ALICE experiment are displayed in Figure 3. The very forward neutral energy flow can be measured by Zero Degree Calorimeters (ZDC) located on both

sides of the central barrel at a distance of 116 m. Additional detectors are used for trigger and event classification purposes. First, the scintillator arrays VZERO-A and VZERO-C cover the range $2.8 < \eta < 5.1$ and $-3.7 < \eta < -1.7$, respectively. This detector is read out in 32 segments due to a four- and eightfold segmentation in pseudorapidity and azimuth, respectively. Second, a Forward Multiplicity Detector (FMD) spans the range $1.7 < \eta < 5.1$ and $-3.4 < \eta < -1.7$, respectively. Third, a new detector system ADA/ADC will be available for data taking in Run II. This new system is installed on both sides of the central barrel in the pseudorapidity range $4.8 < \eta < 6.3$ and $-7. < \eta < -4.9$, respectively.

5. J/ψ production at forward rapidity in Pb-Pb collisions

Exclusive photoproduction can be either coherent with the photon coupling coherently to all nucleons, or incoherent with the photon coupling to individual nucleons. Coherent production results in a low transverse momentum of $p_T \sim 60$ MeV/c, with a 20-30 % probability of breakup of the nucleus. In incoherent production, the nucleus breaks up with a resulting transverse momentum of the vector-meson p_T of ~ 500 MeV/c.

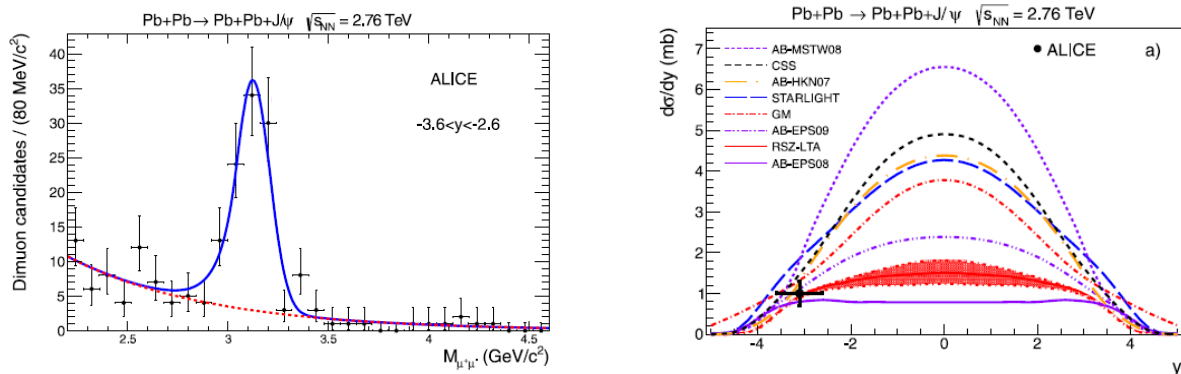


Figure 4. Invariant mass spectrum of two muons of opposite charge on the left, measured coherent cross section on the right with comparison to models (Figures taken from Ref. [9]).

In Figure 4, the two track invariant mass spectrum of events measured in the ALICE muon spectrometer is shown [9]. These events, measured in the Pb-Pb run in the year 2011 with a dedicated trigger, contain exactly two muons of opposite charge, and correspond to an integrated luminosity of about $55 \mu\text{b}^{-1}$. The trigger used here consists of the requirements of a single muon trigger above a p_T -threshold of 1 GeV/c, at least one hit in the VZERO-C detector on the side of the muon spectrometer, and no hit in the VZERO-A detector on the opposite side.

The differential cross section for coherent J/ψ production in the rapidity range $-3.6 < y < -2.6$ derived from this data sample is $d\sigma/dy = 1.00 \pm 0.18$ (stat) $^{+0.24}_{-0.26}$ (syst) mb. On the right hand side of Figure 4, this measured cross section is shown and compared to a number of model predictions. These models differ in the description of the photonuclear interaction. If no nuclear effects are taken into account, then all nucleons participate in the interaction, and the cross section is expected to scale with the number of nucleons squared, i.e. $\sigma \propto A^2$ (AB-MSTW08) [10]. A Glauber approach can be used to calculate the number of nucleons which contribute to the interaction (STARLIGHT, GM, CSS) [11, 12]. In this approach, the reduction in the calculated cross section depends on the J/ψ cross section. In partonic models, the cross section is proportional to the square of the nuclear gluon distribution (AB-EPS08, AB-EPS09, AB-HKN07, RSZ-LTA) [13]. The comparison of the measured cross section to the model calculations shown on the right of Figure 4 clearly shows that all these models give similar predictions at forward rapidity, and hence do not possess much discriminating power at this forward rapidity.

6. J/ψ production at midrapidity in Pb-Pb collisions

During the Pb-Pb run in 2011, a dedicated trigger was running to select events of exclusive production at midrapidity [14]. This trigger consisted of the requirements of at least two hits in the pixel detector of ITS, a number of fired pad-OR (N^{on}) in the TOF detector of $2 \leq N^{on} \leq 6$, and no hits in VZERO detector on either side of the central barrel.

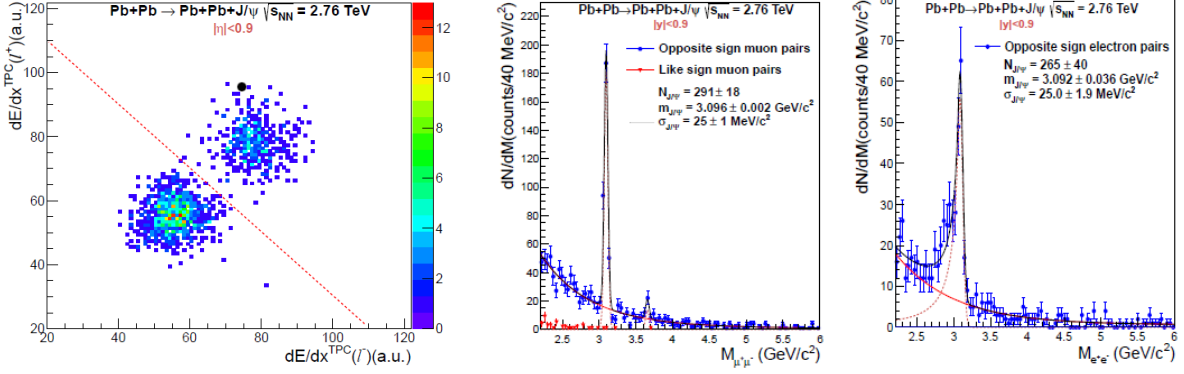


Figure 5. Electron and muon dE/dx signals in the TPC on the left, invariant masses for electron and muon pairs on the right for Pb-Pb collisions at $\sqrt{s_{NN}}=2.76$ TeV (Figures taken from Ref.[14]).

In Figure 5 on the left, the dE/dx signal in the ALICE TPC is plotted for lepton pairs which have an invariant mass in the range $2.8 \leq M_{inv} \leq 3.2$ GeV/c². The signal of the negatively charged lepton of the pair is plotted on the horizontal axis, with the signal of the positively charged lepton on the vertical axis. The two signal areas of electron and muon pairs are clearly separated. On the right hand side of Figure 5, the invariant mass spectra are displayed for electron pairs with transverse momentum $p_T < 300$ MeV/c, and for muon pairs with transverse momentum $p_T < 200$ MeV/c. In the muon channel, the peaks of the J/ψ and $\psi(2S)$ are clearly visible. The mass peak in the electron channel is asymmetric on the low mass side due to bremsstrahlung energy loss while passing through detector material.

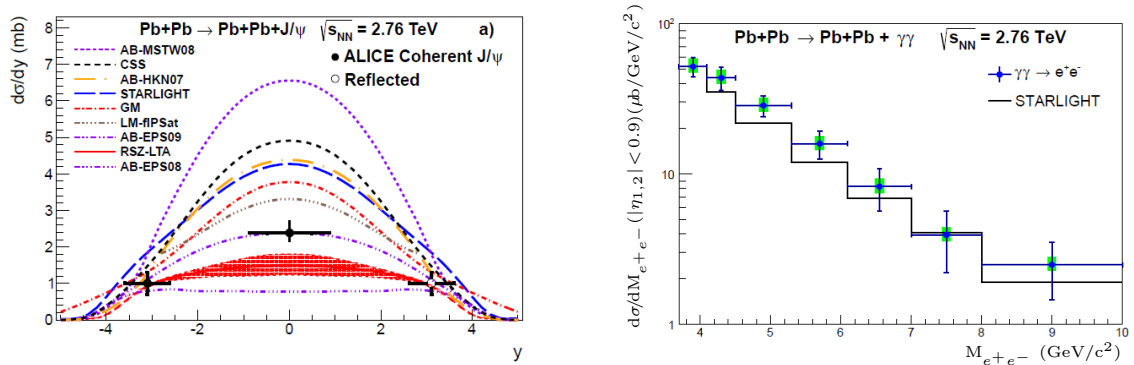


Figure 6. Cross section J/ψ production at midrapidity on the left, cross section $\gamma\gamma \rightarrow e^+e^-$ on the right (Figures taken from Ref.[14]).

The data sample taken with the trigger explained above corresponds to an integrated luminosity of $23 \mu\text{b}^{-1}$. From these data, the cross section value for coherent J/ψ production at midrapidity can be analyzed both in the electron and the muon decay channel, yielding a combined value of $d\sigma_{J/\psi}^{coh}/dy = 2.38^{+0.34}_{-0.24}$ (stat + syst) mb as shown in Figure 6 on the left. The combined value for the incoherent cross section is $d\sigma_{J/\psi}^{incoh}/dy = 0.98^{+0.19}_{-0.17}$ (stat + syst) mb.

From the spectrum shown in Figure 5, the two-photon cross section $\gamma\gamma \rightarrow e^+e^-$ can be extracted by fitting the e^+e^- continuum. This cross section is shown on the right part of Figure 6 for the mass range $3.7 \leq M_{inv} \leq 10 \text{ GeV}/c^2$, and compared to STARLIGHT predictions indicated by the black line [15]. The measured values are about 20% higher than the STARLIGHT predictions, but are compatible within one standard deviation of the data.

7. $\psi(2S)$ production at midrapidity in Pb-Pb collisions

The cross section for exclusive photoproduction of $\psi(2S)$, and comparison to the J/ψ cross section, are of interest since these two states are similar in mass but possess a different radial wavefunction. It is expected that the radial node in the $\psi(2S)$ wavefunction results in a reduced cross section. The same data sample as described above was hence used to extract the coherent cross section for $\psi(2S)$ production [16]. The decay channels $\psi(2S) \rightarrow l^+l^-$ can be extracted from the invariant lepton pair masses as shown in Figure 5 above. In addition, the $\psi(2S)$ can be identified by its decay $\psi(2S) \rightarrow J/\psi \pi^+\pi^-$ with subsequent identification of the J/ψ in the lepton decay channels as explained above.

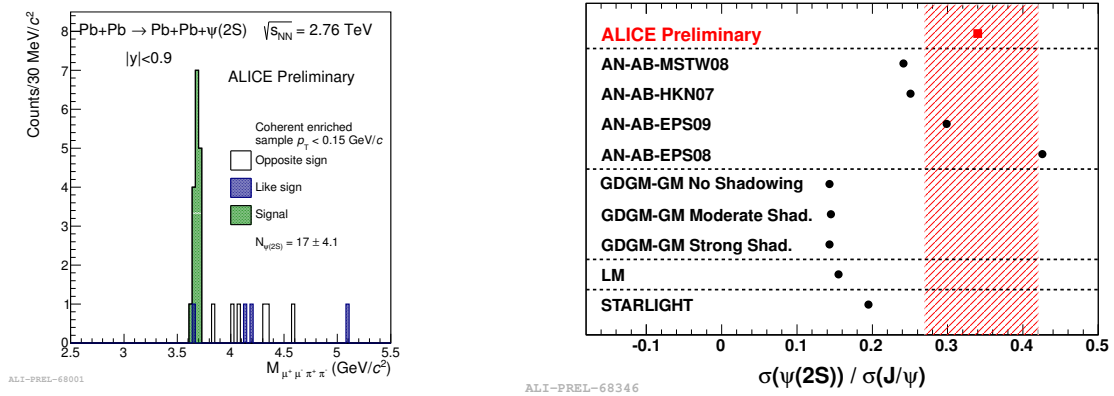


Figure 7. Invariant $\mu^+\mu^-\pi^+\pi^-$ mass spectrum on the left, comparison to models on the right (Figures taken from Ref.[16]).

In Figure 7 on the left, the invariant mass spectrum of $\mu^+\mu^-\pi^+\pi^-$ events is shown. Here, the invariant mass of the muon pair has to meet the requirement of originating from a J/ψ decay. A similar spectrum can be extracted from $e^+e^-\pi^+\pi^-$ events, with the same condition on the electron pair mass of originating from J/ψ decay. From these events, and combined with the direct lepton decay channel, a coherent $\psi(2S)$ cross section is derived for the rapidity interval $-0.9 < y < 0.9$ of $d\sigma_{\psi(2S)}^{coh}/dy = 0.83 \pm 0.19$ (stat+syst)mb.

The ratio of the cross section of J/ψ to $\psi(2S)$ is of particular interest since many of the systematic uncertainties cancel out. The ratio of these two cross sections is derived to be $(d\sigma_{\psi(2S)}^{coh}/dy)/(d\sigma_{J/\psi}^{coh}/dy) = 0.34_{-0.07}^{+0.08}$ (stat+syst). This cross section ratio is shown in Figure 7 on the right, and compared to model predictions.

The model by Adeluyi and Nguyen (AD) makes different predictions based on the different nuclear gluon PDF as defined in EPS08, EPS09, HKN07 and MSTW08 [17, 18, 19, 20]. The model of Gay-Ducati, Griep and Machado (GDGM) is based on colour dipole model [21], as well as the predictions by Lappi and Mantysaari [22]. STARLIGHT uses Vector Dominance model and a parameterization of existing HERA data [23]. Most of these models miss this cross section ratio by a factor of 2-2.5. It is surprising that the AN model seems to describe the data best, even though it assumes an identical wavefunction for the J/ψ and $\psi(2S)$ states.

8. ρ -production at midrapidity in Pb-Pb collisions

The study of ρ -photoproduction is interesting for a variety of reasons. First, this reaction enables the study of a diffractive process at a soft scale, a region where perturbative QCD has little predictive power. Data on ρ -photoproduction from the WA4 experiment at CERN can be well explained by a soft diffractive mechanism up to t -values of a few GeV^2 , i.e. by soft pomeron and f_2, a_2 -exchange [24, 25]. At large t -values $t \sim 100 \text{ GeV}^2$, it is however found that hard pomeron exchange is needed to explain the measured data [7].

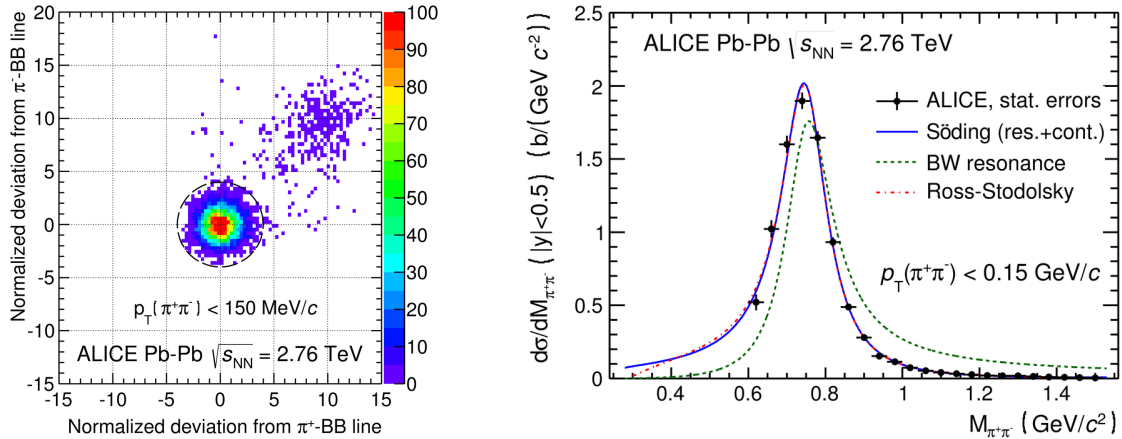


Figure 8. Particle identification from TPC dE/dx on the left, pion pair invariant mass spectra on the right (Figures taken from Ref.[26]).

The data sample for analysing the ρ -photoproduction cross section was recorded by ALICE in the Pb-Pb run in 2010 at an energy of $\sqrt{s_{NN}} = 2.76 \text{ TeV}$ [26]. With the low luminosity at the beginning of the run, a trigger requirement of at least two TOF hits was defined. With increasing luminosity, this requirement was refined to include additionally at least two hits from the pixel layer of the ITS, and no activity in the VZERO counters.

In Figure 8 on the left, the particle identification is shown derived from the dE/dx information of the TPC. On the horizontal axis, the deviation of the measured dE/dx value from the expected dE/dx is shown for the positive pion, with the corresponding quantity for the negative pion on the vertical axis. This deviation is normalized to units of standard deviation. Clearly identified at the origin are $\pi^+\pi^-$ pairs, with e^+e^- pairs from photon-photon interactions located towards the upper right corner.

Figure 8 on the right shows the invariant mass distribution of $\pi^+\pi^-$ pairs. Here, a transverse momentum threshold of $p_T \leq 0.15 \text{ GeV}/c$ is applied for selecting coherent ρ -production. A Breit-Wigner, a Söding and a Ross-Stodolsky parameterization were used to fit the measured ρ -shape. A single Breit-Wigner parameterization shown in Figure 8 by the green dashed line clearly cannot be used to describe the data. The Söding parameterization, taken as the sum of a Breit-Wigner and a continuum contribution, describes the measured data points well. The Ross-Stodolsky function, defined by a Breit-Wigner function multiplied by a mass dependent factor, describes the data also well as indicated in Figure 8 by the blue and red lines.

The analysis of the data taken with the two different triggers discussed above result in cross section values of $11.8 \pm 1.6(\text{stat})_{-1.4}^{+1.1}(\text{syst})\text{mb}$ for the TOF only trigger, and $9.4 \pm 0.7(\text{stat})_{-1.1}^{+0.9}(\text{syst})\text{mb}$ for the TOF-SPD-VZERO trigger.

In the photoproduction process discussed here, additional photons can be exchanged leading to electromagnetic excitation of the Pb-nucleus. This excitation may result in the forward emission of one or several neutrons measured by the ALICE ZDCs. The STARLIGHT and RSZ model show good agreement with the measured neutron multiplicity distribution [27, 13].

9. J/ψ production at forward rapidity in p-Pb collisions

The ALICE collaboration has analysed J/ψ photoproduction in the asymmetric p-Pb system at a nucleon-pair centre-of-mass energy of $\sqrt{s_{NN}} = 5.02$ TeV at forward and backward rapidities [28]. This process can occur on the proton $\gamma + p \rightarrow J/\psi + p$, or on the Pb-nucleus $\gamma + \text{Pb} \rightarrow J/\psi + \text{Pb}$. The much larger photon flux of the Pb-nucleus, however, makes the production on the proton more likely. Such measurements are of high interest since the cross section is sensitive to the gluon PDF at low values of Bjorken- x as explained above. The search for signs of gluon saturation at low- x is one of the open issues of studying QCD. Such signs could, for example, be revealed by studying the cross section of vector-meson photoproduction at the highest collider energies now available, that is at the LHC.

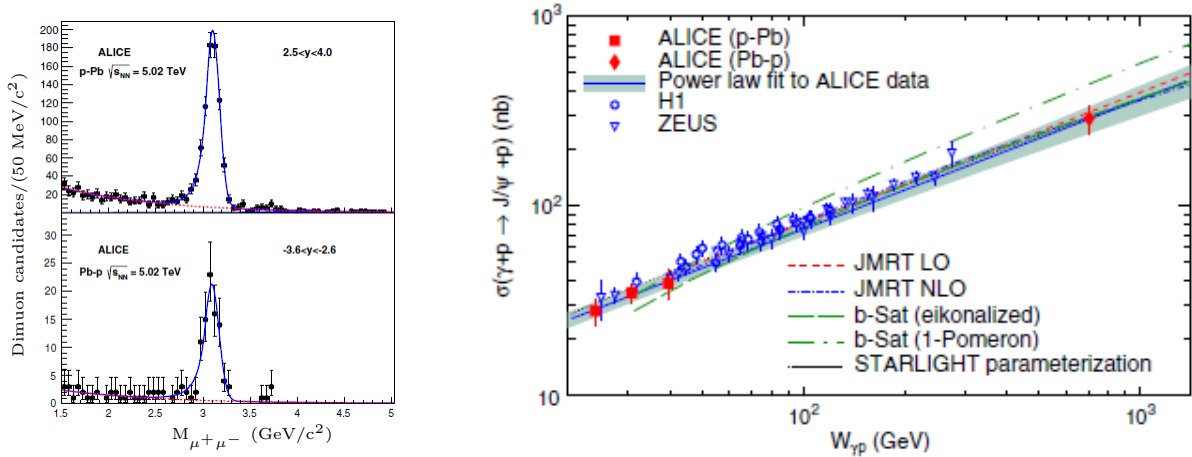


Figure 9. Muon pair invariant mass on the left, J/ψ photoproduction cross section on the right (Figures taken from Ref.[28]).

In Figure 9 on the left, the invariant mass spectrum of muon pairs measured in the muon spectrometer is shown. The direction of the proton and lead beam were reversed in the LHC to be able to measure at forward and backward rapidities, as shown in the upper and lower part of this figure. The measurement of the J/ψ at positive rapidities corresponds to a range of $W_{\gamma p}$ photon-proton center-of-mass energies $21 < W_{\gamma p} < 45$ GeV, whereas negative rapidities correspond to a range of $577 < W_{\gamma p} < 952$ GeV. The muon pair invariant mass spectra at both forward and backward rapidity clearly show a peak due to the J/ψ . The shape of the peak is well described by a Crystal Ball parameterization. The dimuon continuum shown in Figure 9 is fitted with an exponential form as expected to arise from two-photon continuum production.

On the right side of Figure 9, the exclusive J/ψ photoproduction cross section derived from the ALICE data is shown, together with earlier cross section measurements and model predictions. A power law fit to the data measured at HERA yields $\sigma \sim W_{\gamma p}^{\delta}$, with $\delta = 0.69$ and $\delta = 0.67$ for the ZEUS and H1 data, respectively [29, 30]. An analogous fit to the ALICE cross section values yields $\delta = 0.68 \pm 0.06$ (stat+syst). No significant deviation of the power law behaviour of the cross section is hence seen up to energies $W_{\gamma p} \sim 700$ GeV.

The ALICE data shown in Figure 9 are compared to model predictions as follows: The first model, labeled as JMRT LO, is based on a power law description of the process. The second, labeled JMRT NLO, includes next to leading order corrections[31]. Next, the b-Sat predictions are from an eikonalized model using the color glass condensate approach to include saturation[32]. The STARLIGHT parameterization uses a power law fit based on fixed-target and HERA data, yielding $\delta = 0.65 \pm 0.02$. All these predictions agree to the measured data within one sigma of the quoted experimental uncertainty. The b-Sat 1-Pomeron calculation from Ref. [33] is in agreement with the low energy ALICE data points, but is at odds at the high energy data points by about 4 sigmas.

10. New detectors for RUN II

In the shutdown period LS1 between Run I and Run II of the LHC, new detector systems ADA and ADC were installed on A and C-side of ALICE, respectively. These detectors systems consist of double layers of plastic scintillator paddles with light guides coupled to photomultipliers.

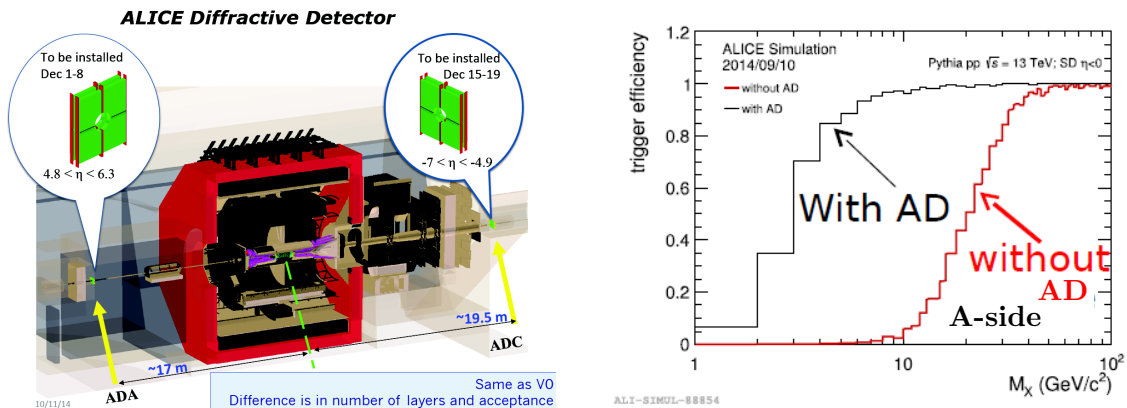


Figure 10. Location of new detectors ADA and ADC in ALICE on the left, trigger efficiency on A-side with and without AD as function of diffractive proton mass M_x on the right.

In Figure 10 on the left, the positions of these new detector systems are shown. The ADA detector, located on A-side of ALICE, covers the pseudorapidity range $4.8 < \eta < 6.3$, with ADC being located on C-side in the range $-7 < \eta < -4.9$. These two systems hence cover approximately two additional units of pseudorapidity on both sides in very forward direction. On the right side of Figure 10, the acceptance on A-side is shown for diffractively excited protons of mass M_x . The threshold for 50% efficiency is lowered from a diffractive mass of about $M_x \sim 20$ GeV/c² to a value of about $M_x \sim 3$ GeV/c². These new detectors will improve the condition of exclusivity in future measurements of exclusive particle production, will extend the acceptance to lower diffractive masses, and will help in rejection of beam-gas background events.

11. Plans for Run II

Run II of the LHC has officially started with the declaration of stable beams on June 3. The present center-of-mass energy in proton-proton mode is $\sqrt{s} = 13$ TeV. It is expected that the LHC will deliver an integrated luminosity of 75-100 fb⁻¹ to the ATLAS and CMS experiments. In the heavy-ion mode of Pb-Pb running, the center-of-mass energy will be $\sqrt{s_{NN}} = 5.1$ TeV. The asymmetric system p-Pb will be measured either at the energy of $\sqrt{s} = 5.1$ or ~ 8 TeV, corresponding to the same energy of the Pb-Pb system, or to the highest energy possible.

12. Summary and outlook

A wealth of information from Run I is available from the ALICE collaboration regarding photon-hadron and photon-photon collisions. The coherent and incoherent J/ψ photoproduction cross section in Pb-Pb collisions has been analysed at midrapidity and at forward rapidity. The coherent $\psi(2S)$ cross section has been examined at midrapidity, and the cross section ratio of these two resonances has been given. The ρ -photoproduction cross section has been presented, and the shape of the ρ invariant mass spectrum has been studied. In addition, the J/ψ photoproduction cross section has been analysed at forward rapidity, and the J/ψ photoproduction cross section has been examined at midrapidity in the asymmetric p-Pb

system. The e^+e^- invariant mass distribution resulting from photon-photon interactions in Pb-Pb collisions has been studied at midrapidity. New detectors systems ADA and ADC have been installed for improved detector coverage at forward rapidities for data taking in Run II.

13. Acknowledgements

This work is supported by the German Federal Ministry of Education and Research under promotional reference 05P15VHCA1.

References

- [1] The ALICE Collaboration, JINST 3 (2008) S08002.
- [2] The ALICE Collaboration, Int.J.Mod.Phys. A29 (2014) 1430044. arXiv:1402.4476.
- [3] E. Fermi, Z.Phys. A29, (1924), 315, doi:10.1007/BF03184853.
- [4] V.M. Budnev, I.F. Ginzburg, G.V. Meledin, V.G. Serbo, Phys.Rept. 15 (1975) 181.
- [5] J.G. Contreras and J.D. Tapia Takaki, Int.J.Mod.Phys. A30 (2015) 1542012.
- [6] G. Wolf, Rept.Prog.Phys. 73 (2010), 116202, arXiv:0907.1217.
- [7] A. Donnachie and P.V. Landshoff, Phys.Lett.B478 (2000), 146, hep-ph/9912312.
- [8] A.D. Martin, C. Nockles, M. Ryskin, T. Teubner, Phys.Lett. B662 (2008), 252, arXiv:0709.4406.
- [9] The ALICE Collaboration, Phys.Lett. B718 (2013) 1273, arXiv:1209.3715.
- [10] A. Adeluyi and C.A. Bertulani, Phys.Rev. C85 (2012) 044904, arXiv:1201.0146.
- [11] V.P. Goncalves and M.V.T. Machado, Phys.Rev. C84 (2011) 011902, arXiv:1106.3036.
- [12] A. Cisek, W. Schäfer and A. Szczurek, Phys.Rev. C86 (2012) 014905, arXiv:1204.5381.
- [13] V. Rebyakova, M. Strikman and M. Zhalov, Phys.Lett. B710, (2012) 647, arXiv:1109.0737.
- [14] The ALICE Collaboration, Eur.Phys.J.C73 (2013) 11, 2617, arXiv:1305.1467.
- [15] <http://starlight.hepforge.org/>.
- [16] The ALICE Collaboration, accepted for publication in Physics Letters B, arXiv:1508.05076.
- [17] K.J. Eskola, H. Paukkunen and C.A. Salgado, JHEP 0807 (2008) 102, arXiv:0802.0139.
- [18] K.J. Eskola, H. Paukkunen and C.A. Salgado, JHEP 0904 (2009) 065, arXiv:0902.4154.
- [19] M. Hirai, S.Kumano and T.-H. Nagai, Phys.Rev. C76 (2007) 065207, arXiv:0709.3038.
- [20] A.D. Martin, W.J. Stirling, R.S. Thorne and G.Watt, Eur.Phys.J.C63 (2009) 189, arXiv:0901.0002.
- [21] M.B. Gay Ducati, M.T. Griep and M.V.T. Machado, Phys.Rev. C88 (2013) 014910, arXiv:1305.2407.
- [22] T. Lappi and H. Mantysaari, Phys.Rev. C87 (2013) 3, 032201, arXiv:1301.4095.
- [23] S. Klein and J. Nystrand, Phys.Rev. C60 (1999) 014903, hep-ph/9902259.
- [24] D. Aston et al., Nuclear Physics B209 (1982) 56.
- [25] A. Donnachie, H.G. Dosch, P.V. Landshoff and O. Nachtmann, *Pomeron Physics and QCD (Cambridge University Press, 2002)*.
- [26] The ALICE Collaboration, JHEP 1509 (2015) 095, arXiv:1503.09177.
- [27] A.J. Baltz, S.R. Klein and J. Nystrand, Phys.Rev.Lett. 89 (2002) 012301, nucl-th/0205031.
- [28] The ALICE Coll., Phys.Rev.Lett. 113 (2014) 23, 232504, arXiv:1406.7819.
- [29] ZEUS Collaboration, Eur.Phys.J. C24 (2002) 345, hep-ex/0201043.
- [30] H1 Collaboration, Eur.Phys.J. C73 (2013) 6, 2466, arXiv:1304.5162.
- [31] S.P. Jones, A.D. Martin, M.G. Ryskin, T. Teubner, JHEP 1311 (2013) 085, arXiv:1307.7099.
- [32] H. Kowalski, L. Motyka and G. Watt, Phys.Rev. D74 (2006) 074016.
- [33] J.L.Abeleira Fernandez et al., arXiv:1211.4831.